International Journal of Microwave and Wireless Technologies

cambridge.org/mrf

A planar triple-band monopole antenna loaded with an arc-shaped defected ground plane for WLAN/WiMAX applications

Shiquan Wang, Fanmin Kong, Kang Li and Liuge Du

School of Information Science and Engineering, Shandong University, 72 Binhai Road, Qingdao 266237, China

Research Paper

Cite this article: Wang S, Kong F, Li K, Du L (2021). A planar triple-band monopole antenna loaded with an arc-shaped defected ground plane for WLAN/WiMAX applications. *International Journal of Microwave and Wireless Technologies* **13**, 381–389. https://doi.org/10.1017/S1759078720001099

Received: 4 February 2020
Revised: 21 July 2020
Accepted: 22 July 2020
First published online: 20 August 2020

Key words:
Triple-band antenna; defected ground plane; simple structure

Author for correspondence:
Fanmin Kong, E-mail: kongfm@sdu.edu.cn

Abstract

In this paper, a new printed triple-band planar antenna combing two different modified monopoles and an arc-shaped defected ground plane is proposed and studied. The used two simple monopoles consist of a rectangular ring and a rectangular patch attached a straight metal strip. And a compact arc-shaped defected ground structure is proposed and used to excite higher resonance frequency and improve the impedance matching of the antenna at lower and middle resonance frequencies. The main radiation element of the proposed antenna composed of only two simple monopoles can support three omnidirectional radiation modes at three desired bands. To indicate the working mechanism of the antenna, the design process is illustrated and the parametric studies are carried out. The experimental results of the fabricated prototype confirm that the triple-band antenna has better radiation efficiencies, appropriate gains, and stable omnidirectional radiation patterns. And the tested results also show that the antenna can provide enough bandwidths of 2.35–2.52, 3.2–4.16, and 5.13–5.87 GHz to cover all the desired 2.4/5.2/5.8 GHz WLAN and 3.5/5.5 GHz WiMAX operations. Moreover, the presented antenna has a very simple structure. Thus, the designed antenna has high practicality and broad prospects for WLAN and WiMAX applications.

Introduction

Multi-band antennas are receiving more and more attention in modern wireless communication systems due to their ability to reduce the number of required antennas, save the space of wireless systems, and lower the cost. In recent years, various multi-band antennas for wireless system applications were presented. The methods of achieving the multi-band designs are diverse, such as loading various slots (L-shaped, U-shaped, etc.) [1–5], adding multiple resonant arms [6–9], using metamaterial structures [10–13], and adopting novel feeding techniques [14–16]. A triple-band dielectric resonator antenna for WLAN and WiMAX applications was designed by Sahu *et al.* [17]. The antenna can obtain different radiating modes by using a modified feeding structure composed of an annular ring patch and a V-shaped printed line. By employing a three-layer substrate and a complex coupled resonators network, Mao *et al.* [18] presented a directional antenna with four working bands applied to wireless applications. In order to achieve the multi-band performances, Weng *et al.* [19] proposed an H-shaped fractal antenna based on the fractal theory for operating over the WLAN and WiMAX bands. This triple-band antenna has well omnidirectional in the lower band and strong directional in the middle and upper bands. Anguera *et al.* [20] proposed a multi-band and small coplanar antenna system applied to handheld wireless communications. The multi-band characteristic of the antenna system was obtained by loading four non-resonant pad elements with different size. And the size of the antenna was greatly reduced by employing ground plane radiation modes. By stacking two dielectric resonators with different permittivities, Khan *et al.* [21] proposed a high-profile antenna with two operating bands for LTE applications. A compact printed monopole antenna with a defected ground plane for Internet of things was presented by Mao *et al.* [22]. The dual-band characteristic of the antenna was produced by the combination of a U-shaped stub and an L-shaped stub as well as a reduced rectangular ground plane. Saurav *et al.* [23] introduced a triple-band dipole antenna loaded with composite right/left-handed unit cell. The three operating bands were obtained by adding two complementary split-ring resonators with different sizes. In [24], Wang *et al.* designed a dual-band and low-profile printed antenna for WiFi and WiGig communications. A compact microstrip resonance battery (CMRC) structure is proposed for feeding monopole in WiFi band and isolating monopole in WiGig band, respectively. Abdalla *et al.* [25] presented a compact quad-band monopole antenna. The multi-band characteristic of the antenna was achieved by etching several composite left- and right-hand (CRLH) structures with different sizes on the rectangular monopole. In [26], Anguera *et al.* summarized the evolution of wireless handheld technologies. And the methods to achieve multi-band design were also introduced, such as adding

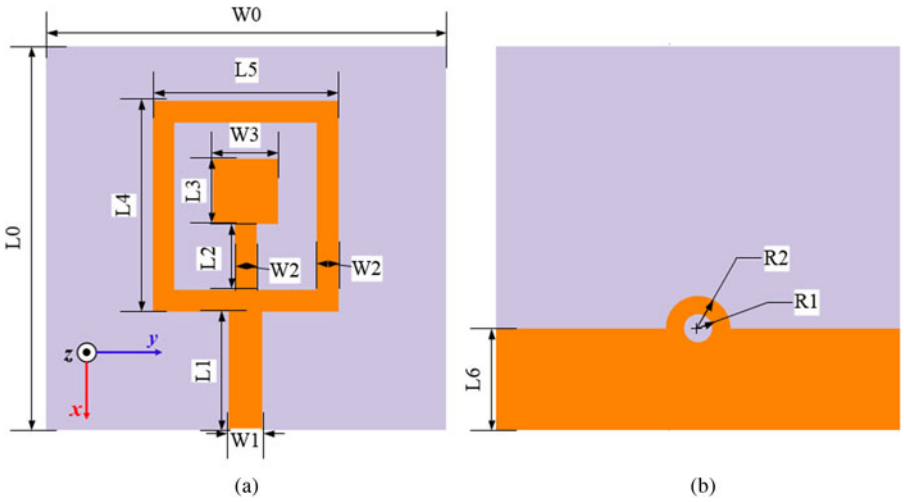

Fig. 1. Geometry of the proposed triple-band antenna, (a) front view, (b) back view.

Table 1. The detailed dimensions for various parameters.

Parameter	Size (mm)	Parameter	Size (mm)
L_0	36	W_3	6
W_0	39	L_4	19.3
L_1	11.4	L_5	17.1
W_1	3.1	L_6	9.3
L_2	5.6	R_1	1.3
W_2	2	R_2	3
L_3	6		

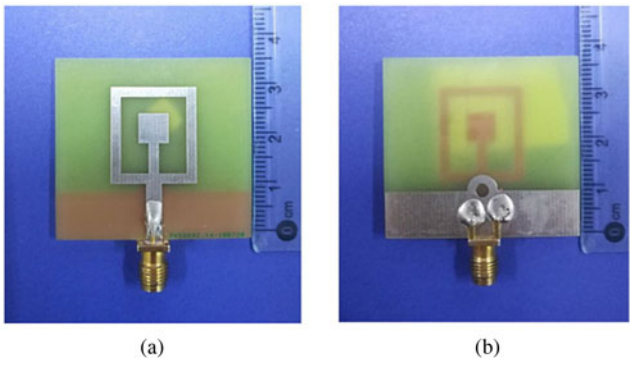

Fig. 2. Prototype of the fabricated antenna, (a) front view, (b) back view.

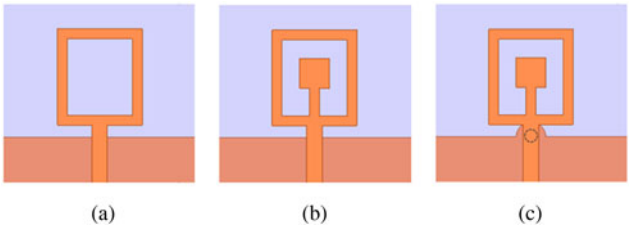

Fig. 3. Design process of the proposed antenna, (a) Antenna-1, (b) Antenna-2, and (c) Antenna-3.

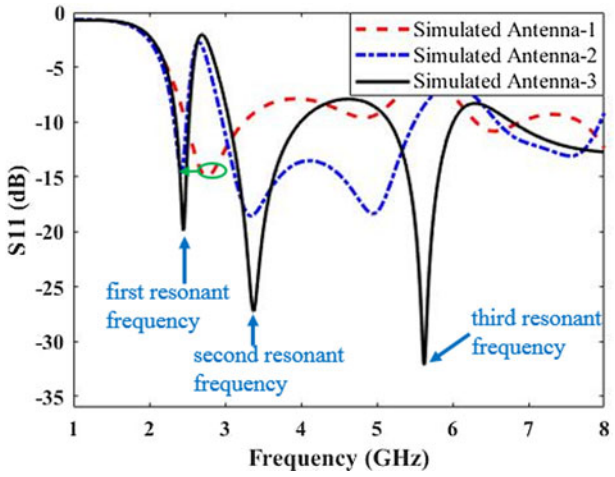

Fig. 4. Simulated reflection coefficients for the three antennas.

multiple monopole parasitic elements and combing planar inverted-F antenna (PIFA) with slots. Although many multi-band antennas with different structures have been proposed, some of the presented antennas do not have sufficient bandwidth to over more WLAN and WiMAX applications and some designs fail to perform stable omnidirectional radiation patterns or reliable gains. Moreover, in order to facilitate processing and cost savings, the multi-band antennas should have a simpler structure. Therefore, a multi-band antenna for WLAN and WiMAX applications with enough bandwidths, stable omnidirectional radiation patterns, reasonable gains and simple structure is desirable.

In this article, a printed triple-band planar antenna for WLAN and WiMAX applications combing different monopoles and defected ground plane is designed. The monopoles compose of a rectangular ring and a rectangular patch attached a straight metal strip, which can generate the lower- and middle-frequency bands and omnidirectional radiation patterns. In order to excite higher resonance frequency and improve the impedance matching of the antenna at lower and middle resonance frequencies, a novel compact arch-shaped ground structure is proposed and used. The presented triple-band antenna has a symmetrical and very simple

https://doi.org/10.1017/S1759078720001099 Published online by Cambridge University Press

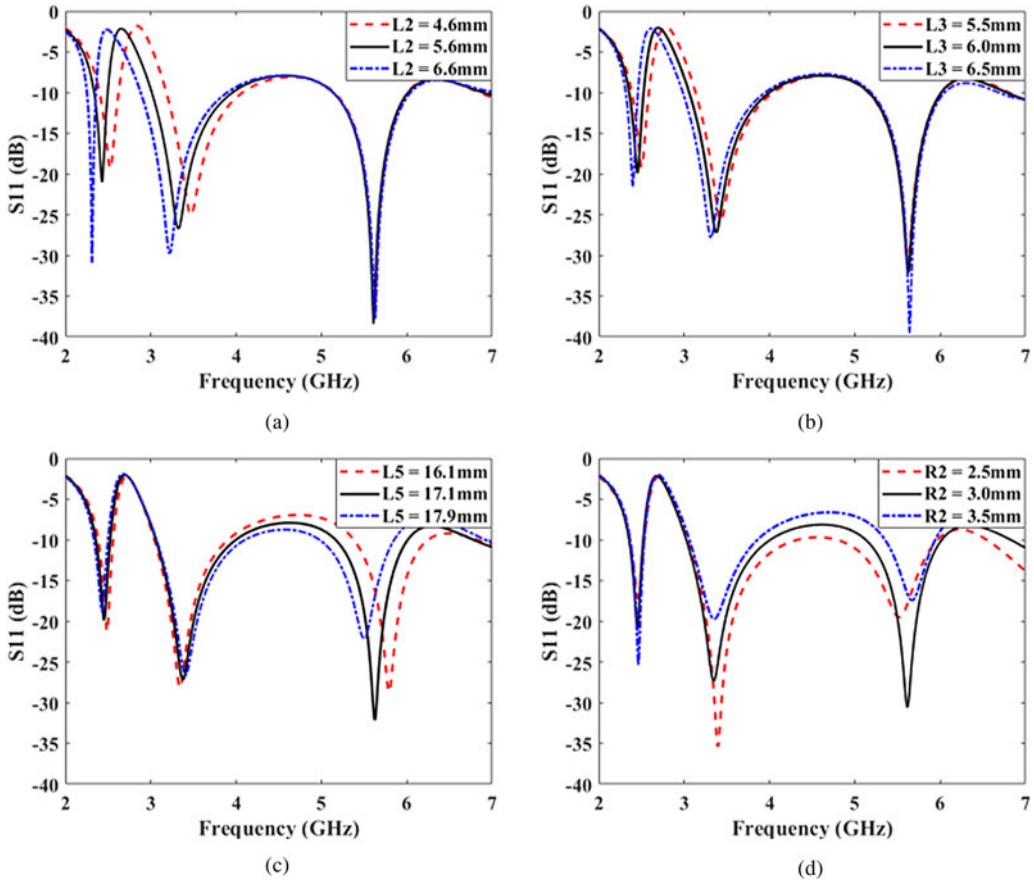

Fig. 5. Simulated reflection coefficients for the antenna with different values of (a) L_2, (b) L_3, (c) L_5, and (d) R_2.

structure. A prototype of the antenna has been fabricated and tested, and the results show that the proposed antenna has three operating bands with enough bandwidths which can cover all the desired 2.4/5.2/5.8-GHz WLAN (2.4–2.48/5.15–5.35/5.725–5.825 GHz) and 3.5/5.5-GHz WiMAX (3.4–3.69/5.25–5.85 GHz) bands. Moreover, the measured results confirm the antenna has consistent omnidirectional radiation patterns and reliable gains in three operating bands.

In the next section, the design details of the antenna are introduced. Later, the effects of important structural parameters and the simulated and measured results are deeply discussed in the section "Parametric analysis" and the section "Results and discussions", respectively. Finally, the section "Conclusions" gives a concise conclusion.

Antenna design

Different schematic views of the designed triple-band antenna are illustrated in Fig. 1. The simple antenna composes of a rectangular ring, a rectangular patch attached a straight metal strip, and an arch-shaped ground plane etched a circular defect. The design selects the 1.6-mm thick FR-4 (relative permittivity $\varepsilon_r = 4.4$, loss tangent $\delta = 0.02$) as the substrate. The compact size of the radiation element is $0.145\,\lambda_0 \times 0.158\,\lambda_0$ (λ_0 is the wavelength in free-space at 2.45 GHz). The presented antenna is fed by a microstrip line with width (W_1) of 3.1 mm. The dimensions of all parameters have been optimized and are listed in Table 1. A prototype of the triple-band antenna is fabricated and its different views are shown in Fig. 2.

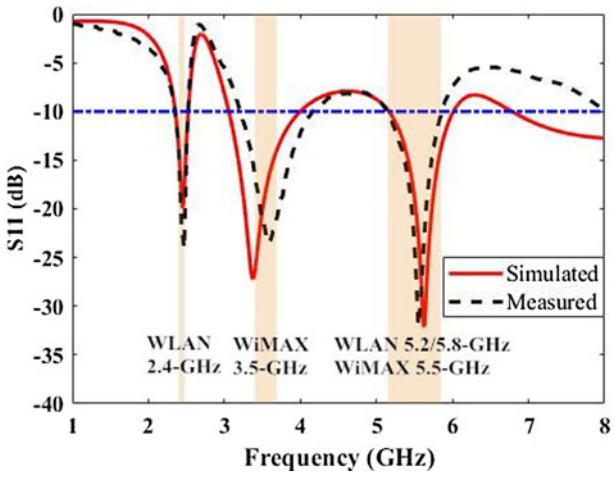

Fig. 6. Simulated and measured reflection coefficients of the antenna.

The antenna design process is depicted in Figs 3 and 4 gives the corresponding simulated reflection coefficients. From Fig. 3(a), it can be seen that the antenna-1 is a simple monopole antenna composed of a modified rectangular ring, which is fed by a 50 Ω microstrip line. The length of half of the rectangular ring ($L_4 + L_5 - 2 \times W_2$) is calculated and optimized to half of the wavelength to excite the first resonance frequency of the antenna-1. And the width of the strips of the rectangular ring (W_2) is set to 2 mm to achieve a good impedance matching of the antenna. Moreover, due to

https://doi.org/10.1017/S1759078720001099 Published online by Cambridge University Press

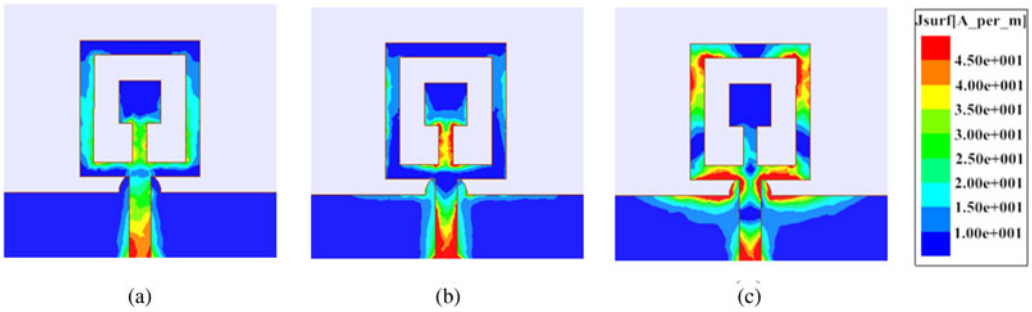

Fig. 7. Simulated current distributions on the antenna at (a) 2.45 GHz, (b) 3.5 GHz, and (c) 5.55 GHz.

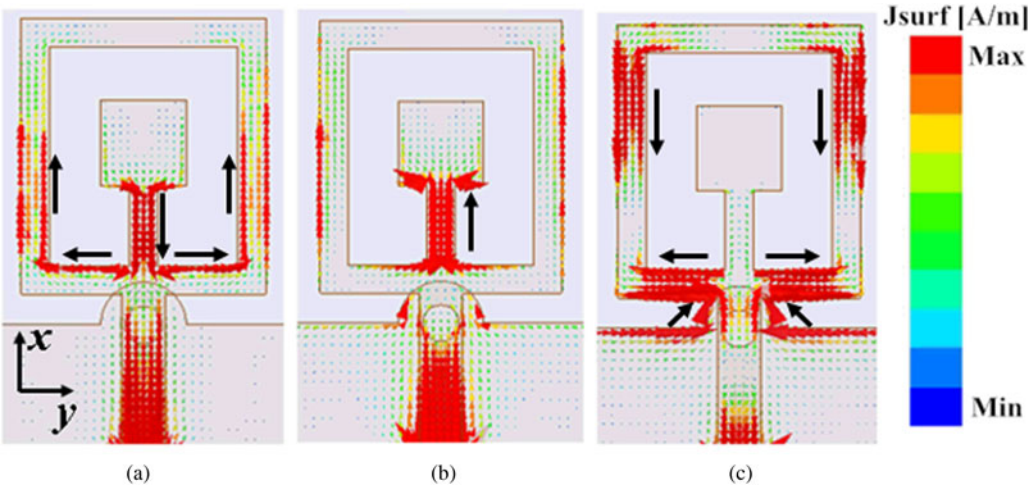

Fig. 8. Simulated vector distributions of the surface current at three different frequencies of (a) 2.45 GHz, (b) 3.5 GHz, and (c) 5.55 GHz.

the rectangular ring fed symmetrically by the microstrip line, the far-field radiation generated by the rectangular ring is mainly determined by the two long strips of the rectangular ring (which length is L_4). Thus, the length of L_4 is adjusted and optimized to obtain a relatively better far-field radiation performance. As demonstrated in Fig. 4, antenna-1 with operating bands of 2.48–3.26 GHz resonates at 2.84 GHz. The first resonant frequency of antenna-1 generated by the rectangular ring and is given by Equation 2. For the first resonance of antenna-1, the length of the current path is half of the guided wavelength.

$$L_{c1} = L_4 + L_5 - 2 \times W_2, \tag{1}$$

$$f_1 = \frac{c}{2 \times \sqrt{\varepsilon_{eff}} \times L_{c1}}, \tag{2}$$

where $\varepsilon_{eff} \approx \varepsilon_r + 1/2$ and c is the speed of light.

By introducing a rectangular patch into the rectangular ring, Antenna-2 is obtained. Adding the rectangular patch to the inside of the rectangular ring allows the antenna to obtain a new resonant frequency and a compact structure. And the dimension of the rectangular patch attached a straight strip is carefully calculated and optimized. From Fig. 4, it can be found that antenna-2 has two operating bands of 2.33–2.49 and 2.97–5.5 GHz which resonate at 2.45 and 3.5 GHz, respectively. The impedance matching of antenna-2 can be realized by adjusting the sizes of the rectangular patch attached a straight strip and the rectangular ground plane. Moreover, it can also be seen that the first resonant frequency excited by antenna-1 is shifted to the left. Thus, it can be summarized that the rectangular patch plays the dual role of generating the second band and adjusting the first band. The left shift of the first resonance is due to the addition of a rectangular patch attached a straight strip, which extends the length of the current path. For the second resonant frequency of the antenna-2, the length of the current path should be a quarter of the guided wavelength, and it can be calculated by Equation (4) approximately.

$$L_{c2} = L_2 + L_3 + (W_3 - W_2)/2, \tag{3}$$

$$f_2 = \frac{c}{4 \times \sqrt{\varepsilon_{eff}} \times L_{c2}}. \tag{4}$$

Further, in order to generate the third operating band of the antenna to cover the desired operations, a circular defect is introduced in the arc-shaped ground plane (Antenna-3). The novel arc-shaped defected structure can be used to effectively adjust the input impedance and impedance matching of the antenna. According to the results of reflection coefficient shown in Fig. 4, the defected structure successfully excites the third resonant frequency and also improves the impedance matching of the first and second resonant frequencies. For antenna-3, the upper

https://doi.org/10.1017/S1759078720001099 Published online by Cambridge University Press

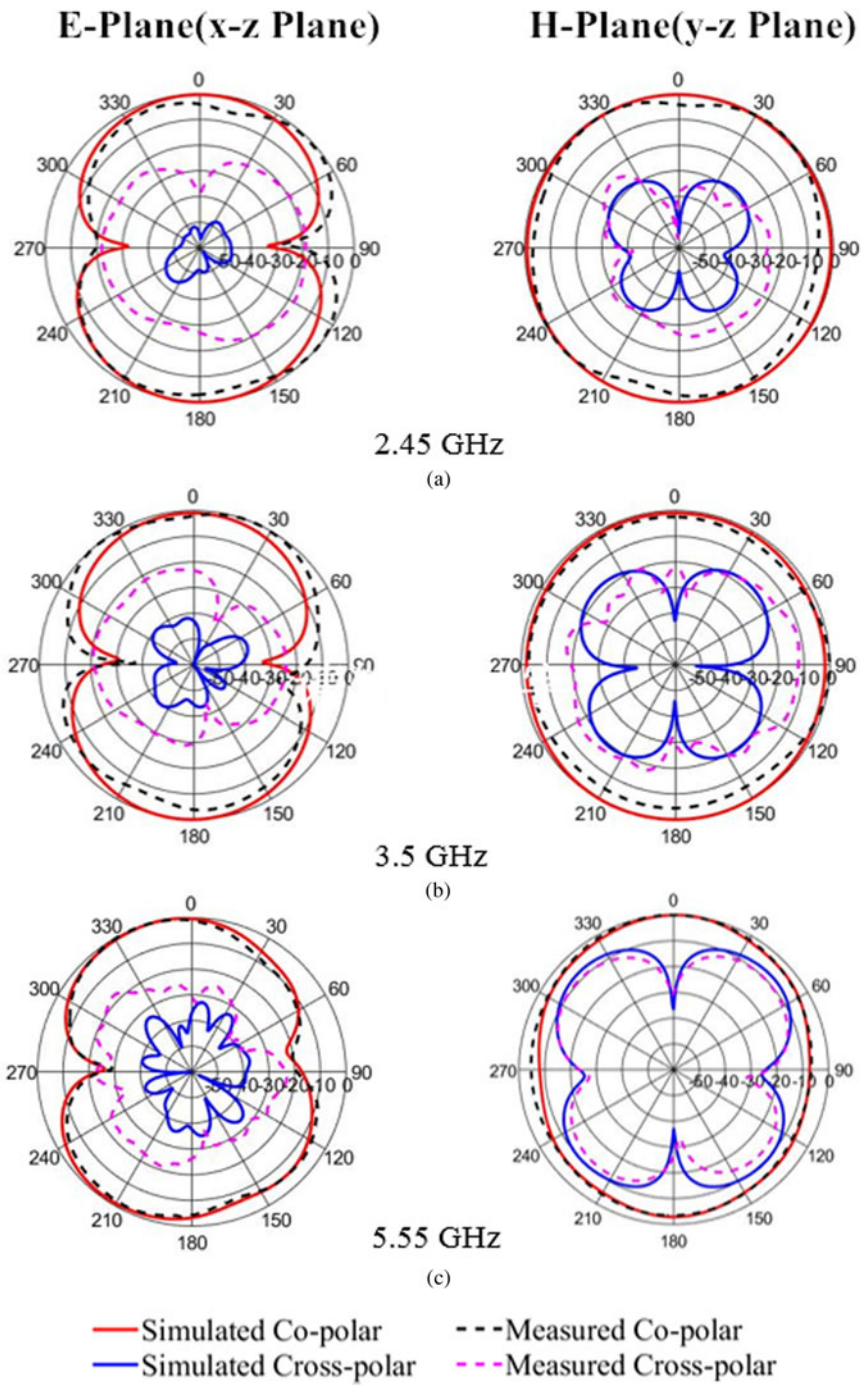

Fig. 9. Simulated and measured radiation characteristics for the antenna at (a) 2.45 GHz, (b) 3.5 GHz, and (c) 5.55 GHz.

band shifts with the change of the dimension (L_6) of the reduced ground plane loaded with defected structure. When the value of L_6 is optimized as 9.3 mm, the upper band of the antenna can cover all the desired 5.2/5.8-GHz WLAN and 5.5-GHz WiMAX operations. Thus, the antenna-3 obtains three working bands of 2.33–2.49, 3.01–3.96, and 5.14–6.01 GHz, which can satisfy the bandwidth requirements of 2.4/5.2/5.8-GHz WLAN and 3.5/5.5-GHz WiMAX operations.

Parametric analysis

To better analyze the operating principle of the antenna, the effects of the rectangular patch, rectangular ring, and defected ground plane on antenna performance are investigated. The studies are done by changing the values of L_2, L_3, L_5, and R_2, while keeping other parameters constant.

Figure 5(a) displays the simulated reflection coefficients for different values of L_2. It can be observed that, with an increase of L_2, the lower and middle bands shift left while the upper band is unchanged. Similarly, both the lower and the middle bands can also be adjusted by tuning the value of L_3. From Fig. 5(b), it is clear that on increasing the value of L_3, a left shift in the lower and middle bands are achieved while the upper band is unaffected. Thus, the desired lower and middle bands for 2.4-GHz WLAN and 3.5-GHz WiMAX operations can be obtained by selecting L_2 as 5.6 mm and L_3 as 6.0 mm.

https://doi.org/10.1017/S1759078720001099 Published online by Cambridge University Press

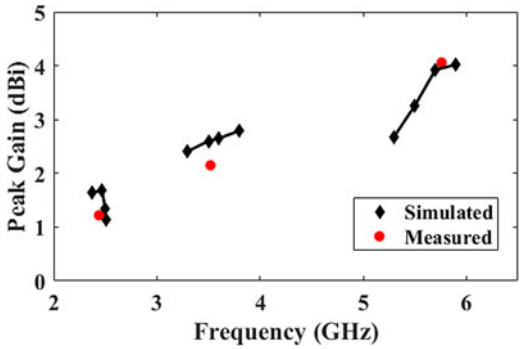

Fig. 10. Simulated and measured peak gains of the triple-band antenna.

Figure 5(c) illustrates the variation of the reflection coefficients by changing the value of L_5. From the figure, it can be seen that, by increasing the value of L_5, the upper bands shift left while the lower and middle bands do not have an obvious movement. Moreover, the effects of the ground plane etched a circular defect on the upper band are also studied by varying parameter $R_2 = 2.5$, 3.0, and 3.5 mm. From Fig. 5(d), with the increasing of R_2, the third resonate frequency shifts to the right and the bandwidth of the upper band is narrowed. Therefore, both L_5 and R_2 can adjust the upper band to cover the 5.2/5.8-GHz WLAN and 5.5-GHz WiMAX bands.

Results and discussions

Reflection coefficients

Figure 6 displays the simulated and measured results of reflection coefficient (S_{11}) for the triple-band antenna. The simulated working frequency bands of the antenna ($|S_{11}|<-10$ dB) are 2.36–2.51 (6.2%), 3.05–4.01 (27.2%), and 5.13–6.01 GHz (15.8%), and the measured three operating bands are 2.35–2.52 (7%), 3.2–4.16 (26.1%), and 5.13–5.87 GHz (13.5%), respectively. Thus, the antenna has enough bandwidths to cover all the desired 2.4/5.2/5.8-GHz WLAN and 3.5/5.5-GHz WiMAX operations. It is able to be seen that the simulated and measured curves have a good agreement. The slight difference between the simulated and measured reflection coefficients (S_{11}) mainly due to the tolerances of the relative permittivity (ϵ_r), poor welding, and the difference between the characteristic impedance of the microstrip feed line of the antenna and the SMA connector.

Surface current distributions

The simulated amplitude and vector distributions of the surface current at three frequencies of 2.45, 3.5, and 5.55 GHz are depicted in Figs 7 and 8. From Fig. 7(a), it can be observed that the surface current is mainly distributed on the rectangular ring and the rectangular patch attached a straight strip. It is able to be concluded that the combination of the rectangular ring and the rectangular patch attached a straight strip generates the lower operating band. As the rectangular ring is fed symmetrically by the microstrip line, the currents on the short strip of the rectangular ring (along the y-axis) have opposite directions on both sides of the feed point as shown in Fig. 8(a). Thus, the far-field radiation patterns and gains at lower band are mainly determined by the current superposition of the currents distributed on the two long strips of the rectangular ring (along the x-axis) and the patch attached a straight strip. However, the currents distributed on the long strips of the rectangular ring and the rectangular patch attached a strip have opposite directions, which causes the surface currents to be partially cancelled and the gains to be relatively weakened at the lower band. At 3.5 GHz, it is found that the current is focused on the rectangular patch attached a straight strip. There is no doubt that the middle frequency band is excited by the rectangular patch attached a straight strip. And the current distributed on the patch attached a straight strip also determines

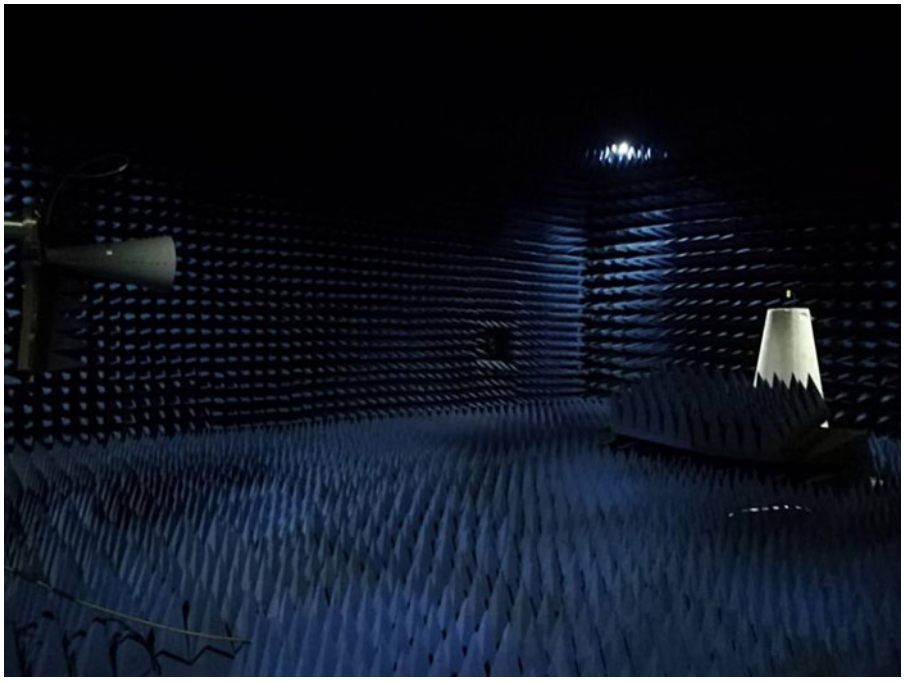

Fig. 11. The photograph of the measurement environment for the presented antenna.

https://doi.org/10.1017/S1759078720001099 Published online by Cambridge University Press

the far-field radiation characteristics of the antenna including radiation patterns and gains at middle band. From Fig. 7(c), it can be observed that, at upper-frequency band, both the rectangular ring and the circular defected structure have higher current density. The rectangular ring and the defected structure play a significant role in the production of the upper operating band. As shown in Fig. 8(c), the currents on the short strip of rectangular ring also have opposite directions on both sides of the feed point. The far-field radiation patterns and gains at upper band mainly generated by the current distributed on the two long strips of the rectangular ring, although the arc-shaped defected structure also has a slight impact on the far-field radiation. Therefore, it can be concluded that the distribution of the surface current and the main radiation element change with frequency. And at lower band, the amplitude of the surface current in the main radiation element is obviously lower than that of the upper band. As a result, the gains are relatively low at lower frequency band compared to the upper frequency.

Radiation characteristics

Figure 9 displays the simulated and measured radiation characteristics of the antenna at 2.45, 3.5, and 5.55 GHz. It is clearly observed that the proposed antenna has bidirectional patterns in the *E*-plane (*x*–*z* plane) and omnidirectional radiation patterns over all three operating frequency bands in the *H*-plane (*y*–*z* plane). And the levels of cross-polarization are lower than that of co-polarization in the *E*- and *H*-plane. The differences between the simulated and measured radiation patterns may be due to the scattering caused by the testing cable, SMA connector and antenna holder, and the chamber scattering. The simulated and tested peak gains of the antenna in three operating bands are drawn in Fig. 10. The simulated peak gains of the antenna are 1.14–1.69, 2.41–2.79, and 2.68–4.02 dBi in 2.37–2.51, 3.3–3.8, and 5.3–5.9 GHz, respectively. And the measured peak gains are 1.22, 2.15, and 4.06 dBi in 2.45, 3.5, and 5.55 GHz, respectively. Moreover, it can be found that the simulated average gain of the upper band is higher than that of middle and lower bands, while the simulated gains at the middle and lower bands are relatively stable. The simulated radiation efficiencies of the antenna are 83–93%, 98–99%, and 92–95% at 2.35–2.48, 3.4–3.65, and 5.15–5.8 GHz, respectively. And the simulated average radiation efficiencies are 88, 98.6, 93.7% in three desired operating bands. The measured radiation efficiencies are roughly 85, 95, and 91 at 2.45, 3.55, and 5.5 GHz, respectively.

The radiation characteristics of the antenna are measured in the anechoic chamber, and Fig. 11 shows its actual environment for far-field measurements. The overall size of the rectangular anechoic chamber is 8 m (length) × 6 m (width) × 3.5 m (height). In the measurement of the proposed antenna, the distance between the auxiliary transmitting antenna and the antenna under test (AUT) is selected as 5 m which can satisfy the requirements of far-field measurements. The equipment used to characterize the antenna in the anechoic chamber is mainly composed of the auxiliary transmitting antenna, vector network analyzer, and test turntable.

Table 2 shows the comparison of the proposed antenna with some multi-band antennas introduced in the literature. From Table 2, it can be concluded that the proposed triple-band antenna provides better radiation efficiency and appropriate gains in a simple structure for all the 2.4/5.2/5.8-GHz WLAN and 3.5/5.5-GHz WiMAX applications.

Table 2. Comparison of the designed antenna with other referred multi-band antennas.

Ref.	Antenna dimensions (λ_0^2)	Structural complexity	Number of bands	Resonant frequencies (GHz)	WLAN bands (GHz)	WiMAX bands (GHz)	Measured gains (dBi)	Efficiencies (%) Simulated	Efficiencies (%) Measured	Stable omni-directional patterns
[4]	0.420 × 0.270	Medium	Triple	2.45, 3.5, 5.35	2.4/5.2	3.5	−0.9, 1.8, −1	N.A.	N.A.	No
[6]	0.275 × 0.142	Medium	Dual	2.5, 3.5, 5.5	2.4/5.2/5.8	3.5/5.5	1, 1.6, 2.3	65, 70, 55	N.A.	Yes
[7]	0.083 × 0.083	Simple	Triple	1.78, 3.52, 5.2	5.2	3.5	Peak Gain 2.7	N.A.	N.A.	Yes
[12]	0.304 × 0.304	Medium	Triple	1.9, 2.45, 5	2.4/5.2	2.5	1.64, 2.07, 4.06	N.A.	66, 77, 88	Yes
[14]	0.292 × 0.267	Medium	Triple	2.5, 3.5, 5.5	2.4/5.8	3.5/5.5	0.7, 0, 1.6	86, 89, 90	N.A.	Yes
[17]	0.350 × 0.350	Complex	Triple	2.1, 3.61, 6.16	5.2/5.8	3.5/5.5	1.2, 2.9, 3.5	N.A.	N.A.	No
[19]	0.852 × 1	Complex	Triple	2.5, 3, 5.2	2.4/5.2/5.8	5.5	N.A.	N.A.	N.A.	No
[27]	0.320 × 0.240	Simple	Dual	2.4, 5.3	2.4/5.2/5.8	5.5	1.01, 1.8	84, 90	N.A.	Yes
[28]	0.227 × 0.181	Medium	Quad	1.7, 2.4, 3.1, 4.5	2.4/5.2/5.8	3.5/5.5	1.6, 2.15, 2.75, 3.8	81, 98, 93, 82	78, 96, 92, 80	No
[29]	0.136 × 0.104	Complex	Triple	2.4, 3.5, 5.2	2.4/5.2	3.5/5.5	0.44, 1.59, 2.72	N.A.	68, 82, 84	Yes
[30]	0.290 × 0.254	Complex	Dual	2.48, 3.16	2.4	3.5	1.05, 1.09	N.A.	N.A.	No
This work	0.294 × 0.318	Simple	Triple	2.45, 3.55, 5.5	2.4/5.2/5.8	3.5/5.5	1.22, 2.15, 4.06	88, 99, 94	85, 95, 91	Yes

https://doi.org/10.1017/S1759078720001099 Published online by Cambridge University Press

Conclusions

A new printed triple-band planar antenna combing two different modified monopoles and an arc-shaped defected ground plane for WLAN and WiMAX applications are proposed. By employing two simple modified monopoles of a rectangular ring and a rectangular patch attached a straight strip, the lower and middle operating bands and the omnidirectional radiation patterns are obtained. Furthermore, in order to excite a new resonance at a higher frequency and improve the impedance matching at lower and middle resonance frequencies, a new compact arch-shaped defected ground structure is proposed and used. With the help of the arch-shaped defected ground structure, the main radiation element of the antenna composed of only two simple monopoles provides three omnidirectional radiation modes at three desired bands. And the presented triple-band antenna has a very simple structure. In order to verify the performance of the antenna, a prototype of the triple-band antenna is fabricated and tested. The measured results indicate that the proposed antenna has better radiation efficiencies, stable omnidirectional patterns, and reasonable gains. And the experimental results also show that the antenna provi enough bandwidths to cover all the desired 2.4/3.5/5.2-GHz WLAN and 3.5/5.5-GHz WiMAX applications. Therefore, the several advantages of better radiation efficiency, stable omnidirectional pattern, appropriate gain, enough bandwidth, and simple structure make the proposed triple-band antenna high practicality and good prospect for WLAN and WiMAX applications.

Acknowledgements. This research work was supported by the National Key R&D Program of China under Grant No. 2016YFC0302802, and by the National Natural Science Foundation of China under Grant No. 61475084 and 61801267.

References

1. **Boukarkar A, Lin XQ, Jiang Y and Yu YQ** (2017) Miniaturized single-feed multiband patch antennas. *IEEE Transactions on Antennas and Propagation* **65**, 850–854.
2. **Dhar S, Patra K, Ghatak R, Gupta B and Poddar DR** (2015) A dielectric resonator-loaded Minkowski fractal-shaped slot loop heptaband antenna. *IEEE Transactions on Antennas and Propagation* **63**, 1521–1529.
3. **Keshari JP, Kanaujia BK, Khandelwal MK, Bakariya PS and Mehra RM** (2017) Omnidirectional multi-band stacked microstrip patch antenna with wide impedance bandwidth and suppressed cross-polarization. *International Journal of Microwave and Wireless Technologies* **9**, 629–638.
4. **Bekasiewicz A and Koziel S** (2018) Miniaturized uniplanar triple-band slot dipole antenna with folded radiator. *Microwave and Optical Technology Letters* **60**, 386–389.
5. **Baytore C, Gocen C, Palandoken M, Kaya A and Zoral EY** (2019) Compact metal-plate slotted WLAN-WIMAX antenna design with USB Wi-Fi adapter application. *Turkish Journal of Electrical Engineering and Computer Sciences* **27**, 4403–4417.
6. **Karthikeyan M, Sitharthan R, Ali T and Roy B** (2020) Compact multi-band CPW fed monopole antenna with square ring and T-shaped strips. *Microwave and Optical Technology Letters* **62**, 926–932.
7. **Beigi P and Mohammadi P** (2016) A novel small triple-band monopole antenna with crinkle fractal-structure. *International Journal of Electronics and Communications (AEÜ)* **70**, 1382–1387.
8. **Chen YJ, Liu TW and Tu WH** (2017) CPW-fed penta-band slot dipole antenna based on comb-like metal sheets. *IEEE Antennas and Wireless Propagation Letters* **16**, 202–205.
9. **Alam MJ, Faruque MRI, Hasan MM and Islam MT** (2017) Split quad-rilateral miniaturized multiband microstrip patch antenna design for modern communication system. *IET Microwaves, Antennas and Propagation* **11**, 1317–1323.
10. **Hasan MM, Faruque MRI and Islam MT** (2018) Dual band metamaterial antenna for LTE/bluetooth/WiMAX system. *Scientific Reports* **8**, 1240.
11. **Ali T, Saadh Aw M and Biradar RC** (2018) A fractal quad-band antenna loaded with L-shaped slot and metamaterial for wireless applications. *International Journal of Microwave and Wireless Technologies* **10**, 826–834.
12. **Alam T, Samsuzzaman M, Faruque MRI and Islam MT** (2016) A metamaterial unit cell inspired antenna for mobile wireless applications. *Microwave and Optical Technology Letters* **58**, 926–932.
13. **Gao X, Jackson TJ and Gardner P** (2017) Multiband open-ended resonant antenna based on one ECRLH unit cell structure. *IEEE Antennas and Wireless Propagation Letters* **16**, 1273–1276.
14. **Abdalla MA, Hu Z and Muvianto C** (2017) Analysis and design of a triple band metamaterial simplified CRLH cells loaded monopole antenna. *International Journal of Microwave and Wireless Technologies* **9**, 903–913.
15. **Bakariya PS, Dwari S, Sarkar M and Mandal MK** (2015) Proximity-coupled microstrip antenna for bluetooth, WiMAX, and WLAN applications. *IEEE Antennas and Wireless Propagation Letters* **14**, 755–758.
16. **Zhu J, Antoniades MA and Eleftheriades GV** (2010) A compact tri-band monopole antenna with single-cell metamaterial loading. *IEEE Transactions on Antennas and Propagation* **58**, 1031–1038.
17. **Sahu NK, Sharma A and Gangwar RK** (2017) Modified annular ring patch fed cylindrical dielectric resonator antenna for WLAN/WIMAX applications. *Microwave and Optical Technology Letters* **59**, 120–125.
18. **Mao CX, Gao S, Wang Y and Sanz-Izquierdo B** (2017) A novel multi-band directional antenna for wireless communications. *IEEE Antennas and Wireless Propagation Letters* **16**, 1217–1220.
19. **Weng WC and Hung CL** (2014) An H-fractal antenna for multiband applications. *IEEE Antennas and Wireless Propagation Letters* **13**, 1705–1708.
20. **Anguera J, Andújar A and García C** (2013) Multiband and small coplanar antenna system for wireless handheld devices. *IEEE Transactions on Antennas and Propagation* **61**, 3782–3789.
21. **Khan R, Jamaluddin MH, Kazim JUR, Nasir J and Owais O** (2016) Multiband-dielectric resonator antenna for LTE application. *IET Microwaves, Antennas and Propagation* **10**, 595–598.
22. **Mao YF, Guo ST and Chen MG** (2018) Compact dual-band monopole antenna with defected ground plane for internet of things. *IET Microwaves, Antennas and Propagation* **12**, 1332–1338.
23. **Saurav K, Sarkar D and Srivastava KV** (2014) CRLH unit-cell loaded multiband printed dipole antenna. *IEEE Antennas and Wireless Propagation Letters* **13**, 852–855.
24. **Wang D and Chan CH** (2016) Multiband antenna for WiFi and WiGig communications. *IEEE Antennas and Wireless Propagation Letters* **15**, 309–312.
25. **Abdalla MA and Hu ZR** (2018) Design and analysis of a compact quad band loaded monopole antenna with independent resonators. *International Journal of Microwave and Wireless Technologies* **10**, 479–486.
26. **Anguera J, Andújar A, Huynh MC, Orlenius C, Picher C and Puente C** (2013) Advances in antenna technology for wireless handheld devices. *International Journal of Antennas and Propagation* **2013**, 388–391.
27. **Verma S and Kumar P** (2014) Printed inverted-L shaped monopole antenna with parasitic inverted-F element for dual band applications. *Microwave and Optical Technology Letters* **56**, 1163–1167.
28. **Mark R, Mishra N, Mandalb K, Sarkarc PP and Dasa S** (2018) Hexagonal ring fractal antenna with dumbbell-shaped defected ground structure for multiband wireless applications. *International Journal of Electronics and Communications (AEÜ)* **94**, 42–50.
29. **Kumar P, Dwari S and Bakariya PS** (2017) Compact triple-band stacked monopole antenna for USB dongle applications. *International Journal of RF and Microwave Computer-Aided Engineering* **28**, 1–9.
30. **Singh G, Kanaujia BK, Pandey VK, Gangwar D and Kumar S** (2019) Design of compact dual-band patch antenna loaded with D-shaped complementary split ring resonator. *Journal of Electromagnetic Wave* **16**, 2096–2111.

https://doi.org/10.1017/S1759078720001099 Published online by Cambridge University Press

Shiquan Wang was born in Linyi, China. He received the B.S. degree in electronic information science and technology from Qilu University of Technology (Shandong academy of sciences) in 2017. He is currently pursuing the Ph.D. degree in electronic science and technology with the School of Information Science and Engineering, Shandong University, Qingdao. His current research interests include design and analysis of antennas, microwave devices, and metamaterials.

Fanming Kong received the B.S. and M.S. degrees in electrical engineering from Shandong University, Jinan, China, in 1991 and 1994, respectively, and the Ph.D. degree from the School of Physics, Shandong University, in 1999. He joined the Department of Electrical Engineering, Shandong University, in 1999, where he is currently a Professor with the School of Information Science and Engineering. His current research interests include design and analysis of antennas, microwave integrated circuits, and computational electromagnetics.

Kang Li was born in Jinan, China, in 1962. He received the B.S. and M.S. degrees in electrical engineering and the Ph.D. degree in optical engineering from Shandong University, Jinan, in 1984, 1987, and 2006, respectively. He is currently a Professor with the School of Information Science and Engineering, Shandong University. He is a member of IEEE (USA) and a reviewer of many International and National journals. His current research interests include antennas, computational electromagnetics, and fiber-optic communications.

Liuge Du received the B.S. degree in electronic science and technology and the M.S. and the Ph.D. degrees in radio physic from Shandong University, Jinan, China, in 2005, 2008 and 2011, respectively. From 2011 to 2017, he was an engineer with the 41st research institute of China Electronics Technology Group Corporation (CETC). He is currently an Associate Professor with the electronic science and technology, Shandong University. His interests include design and measurement of antennas, algorithm for microwave imaging, and computational electromagnetics.

https://doi.org/10.1017/S1759078720001099 Published online by Cambridge University Press